

Deterministic coupling of a quantum emitter to surface plasmon polaritons, Purcell enhanced generation of indistinguishable single photons and quantum information processing

Lakshminarayan Sharma¹ and Laxmi Narayan Tripathi*²

*¹Department of Physics, Birla Institute of Technology,
Mesra, Ranchi-835215, Jharkhand, India*

*²Department of Physics, School of Advanced Sciences,
Vellore Institute of Technology, Vellore-632014, Tamilnadu, India**

(Dated: August 26, 2021)

Abstract

Integrated photonic circuits are an integral part of all-optical and on-chip quantum information processing and quantum computer. Deterministically integrated single-photon sources in nanoplasmonic circuits lead to densely packed scalable quantum logic circuits operating beyond the diffraction limit. Here, we report the coupling efficiency of single-photon sources to the plasmonic waveguide, characteristic transmission spectrum, propagation length, decay length, and plasmonic Purcell factor. We simulated the transmission spectrum to find the appropriate wavelength for various width of the dielectric in the metal-dielectric-metal waveguide. We find the maximum propagation length of $3.98 \mu\text{m}$ for Al_2O_3 dielectric-width equal to 140 nm and coupling efficiency to be greater than 82 %. The plasmonic Purcell factor was found to be inversely proportional to dielectric-width (w), reaching as high as 31974 for w equal to 1 nm. We also calculated quantum properties of the photons like indistinguishability and found that it can be enhanced by plasmonic-nanocavity if single-photon sources are deterministically coupled. We further, propose a scalable metal-dielectric-metal waveguide based quantum logic circuits using the plasmonic circuit and Mach-Zehnder interferometer.

INTRODUCTION

Surface plasmon polaritons (SPP) are electromagnetic surface waves coupled to free electron oscillations in metal. They propagate along the metal-dielectric boundary with the transverse amplitude decaying exponentially at both sides [1–3]. The smallest dimension d , to which light can be concentrated is limited by the diffraction, which is $d \geq \lambda/2n$ where λ is the wavelength of the electromagnetic wave, n is the refractive index of the medium. SPPs break the classical diffraction limit [4] and can confine light to a nanoscale length regime which makes them an attractive plasmonic platform for on-chip integrated quantum photonic circuits [5–10]. A diverse type of geometrical structures have been used for SPPs propagation like metal-dielectric-metal (MDM) wave-guides [11–19], slot wave-guides [20–22] and channel plasmon waveguide [23]. With the photonic integrated circuits several numbers of complex optical and electronic circuits can be miniaturized on a single chip [9, 24–26]. Linear optical quantum information processing requires single-photon sources (SPS) [27]. Several SPSs have been identified in

the past decades such as quantum dots [28], transition metal dichalcogenides (TMDC) [29], hBN (hexagonal Boron Nitride) [30, 31], Nitrogen vacancy in diamonds [32], spontaneous parametric down-conversion in nonlinear crystals etc [33]. Recently, it has been found that the coupling of single photons sources with cavity results in Purcell enhanced indistinguishability [34–36].

Metal-dielectric-metal sub-wavelength plasmonic waveguides have been shown as beam splitters and bend [37, 38], directional coupler, and Mach-Zehnder interferometer [39]. As opposed to classical information processing using bits, which is either 0 or 1, quantum information processing involves superposition states [40, 41]. Superposition states imply the probabilistic nature of bits, 0 and 1 (known as quantum bits or qubits). Any measurement for 0 and 1 destroys the superposition state known as the no-cloning theorem [42]. This no-cloning property of the quantum states (superposition states) makes the communication secure. The qubits or 0 and 1 can be realized in single photons by assigning 0 and 1 to orthogonally polarized states usually referred to as polarization qubits [43]. In this case, the horizontal polarization state can be ascribed to 0 and vertical polarization as 1. The polarization qubits of single photons can easily be generated, controlled, and further manipulated by common linear optical devices like waveplates. The single photons thus offer the most prominent source of qubits. A polarization qubit is a coherent superposition of horizontal and vertical polarization-maintaining a certain phase relation among them. Such a qubit is equivalent to a photon polarized at $+45^\circ$. Setting a polarizer at the angle $+45^\circ$ will allow the passing of the photon with 100 % probability and with zero probability at -45° [43] and thus linear optics is very well suited for quantum computation [44, 45]. In this paper, we have investigated the SPP properties such as propagation length, decay length, and the plasmonic Purcell Factor change in Ag- Al_2O_3 -Ag waveguide using Finite Difference Time Domain (FDTD) simulations and analytical calculations. We also calculated Purcell enhanced Indistinguishability of photons for various emitters coupled with a nano-plasmonic cavity. Our integrated SPS and metal-dielectric-metal waveguide system are suitable for scalable plasmonic platform based high-density optical quantum processing circuits. We propose that using linear optical elements, our deterministically placed nanoantenna - coupled single-photon sources and Mach-Zehnder interferometer, a controlled-NOT gate can be formed.

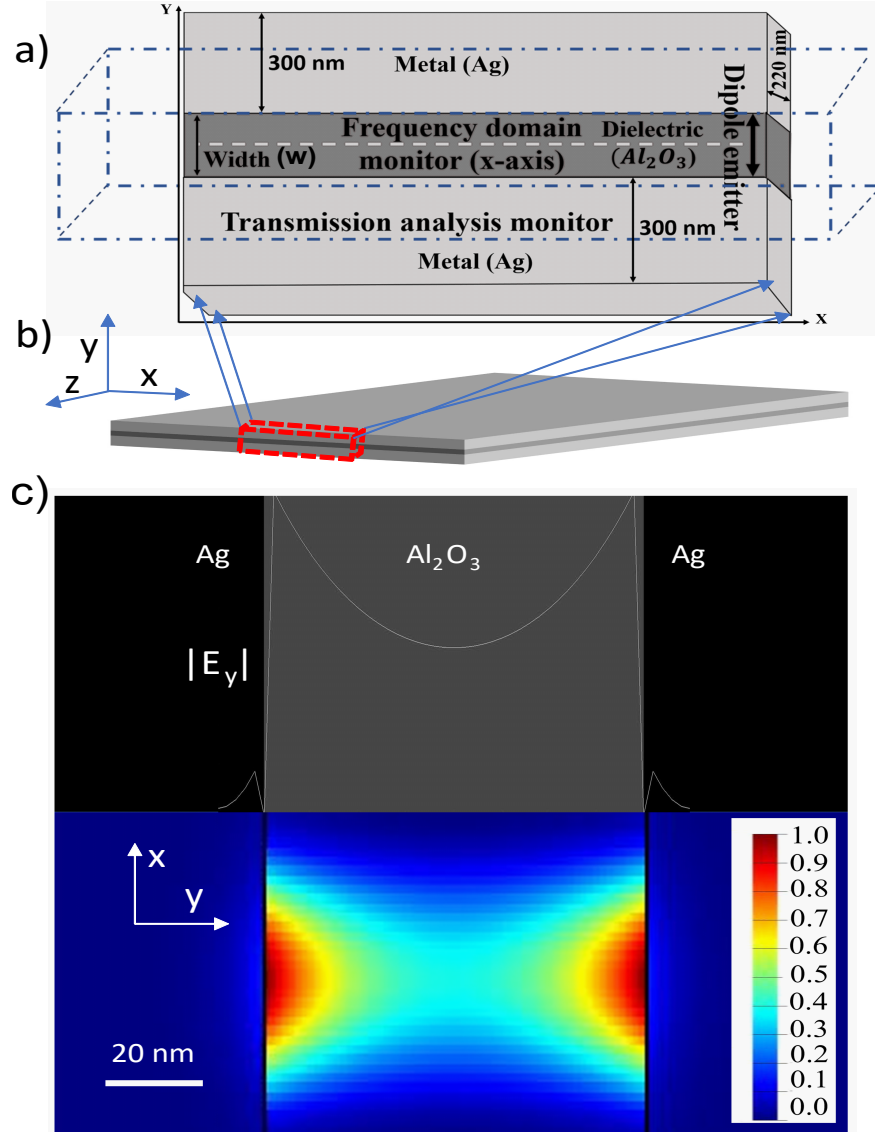


Figure 1. (a) FDTD simulation design of metal-dielectric-metal plasmonic waveguide with dipole emitter (in XY plane) embedded in the Al_2O_3 layer. (b) Thin film based easy to fabricate metal-dielectric-metal waveguide. (c) Top: Transverse E_y -field profile in the waveguide for dielectric-width w equal to 80 nm at λ equal to 437 nm. Bottom: XY cross section of TM1 mode (symmetrical mode) of the MDM waveguide. Color scale: Normalized magnitude of E_y -field.

FINITE DIFFERENCE TIME DOMAIN SIMULATION DESIGN AND THEORETICAL MODEL

Our FDTD simulation MDM waveguide design (Fig. 1) consists of two identical Ag layer of width 300 nm each separated by the dielectric (Al_2O_3) spacer of width w . The horizontal length is equal to $63 \mu\text{m}$ and the z span is 220 nm. Transmission analysis

monitor (dashed cuboid box) was used to find the wavelength of maximum transmission (λ_{max}). The frequency domain monitor (dashed white line passing through the dielectric) was kept along x-axis for measuring the field intensity. The structure was designed and modeled in Lumerical solutions FDTD and MODE software with perfectly matched boundary keeping the mesh size equal to 5 nm. The transmission spectrum for the various dielectric-width ranging from 20 nm to 150 nm in step of 10 nm was recorded to find the wavelength of maximum transmission (λ_{max}). The dielectric function of metals as described by Drude model [46] is

$$\epsilon(m) = 1 - \frac{\omega_p^2}{(\omega^2 + \gamma\omega i)} \quad (1)$$

here ω_p is the plasma frequency and γ is the characteristic collision frequency. The plasma frequency is given as [4]

$$\omega_p = \frac{ne^2}{\epsilon_0 m} \quad (2)$$

where n is density of free electrons, e is electronic charge, ϵ_0 is the permittivity of free space and m is mass of an electron. The value of ω_p the plasma frequency and γ characteristic collision frequency used for Ag are 1.37×10^4 THz [47] and 100 THz [4] respectively and ϵ_d for Al_2O_3 is 9 [48].

ANALYTICAL CALCULATION OF SURFACE PLASMON POLARITON CHARACTERISTICS

For single interface between metal and dielectric, the dispersion relation of SPP is given by [4]

$$K_{SPP} = K_0 \sqrt{\frac{\epsilon_m \epsilon_d}{\epsilon_m + \epsilon_d}} \quad (3)$$

with ϵ_m and ϵ_d equal to dielectric permittivity of metal and dielectric respectively.

For single interface between metal and dielectric the large SPP wave vector value is approached when ω is equal to characteristic surface plasmon frequency ω_{sp} [4]

$$\omega_{sp} = \frac{\omega_p}{\sqrt{1 + \epsilon_d}} \quad (4)$$

ω_{sp} for Ag and Al_2O_3 interface is 4.3×10^3 THz.

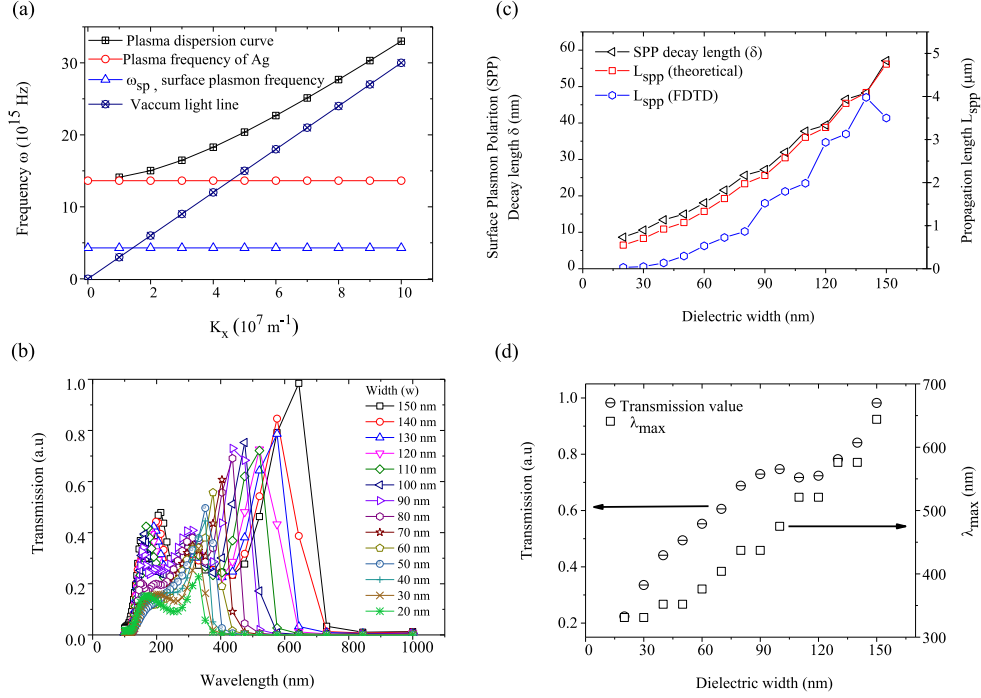


Figure 2. (a) The plasma dispersion curve for silver (Ag), plasma frequency for Ag from equation 2 and the surface plasmon frequency for single interface with Al₂O₃ as the dielectric from equation 4 and the ω vs K relation for light in vacuum. (b) Transmission vs wavelength plot for the various dielectric-width (20 nm - 150 nm). (c) Surface plasmon polariton decay length (δ), calculated surface plasmon polariton propagation length (L_{spp}) and the simulated propagation length (L_{spp}) from FDTD with increasing width of the dielectric layer from 20 nm to 150 nm in steps of 10 nm. (d) The peak transmission wavelength (λ_{max}) and the normalized transmission value plot for changing dielectric-width (w) of the MDM waveguide.

The complex propagation constant for SPP in multilayer system as MDM is given by [49]

$$K_{SPP} = n_{eff}K_0 \quad (5)$$

with

$$n_{eff} = (\epsilon_d)^{1/2} \sqrt{1 + \frac{\lambda}{\pi w (-\epsilon_m)^{1/2}} \left(1 + \frac{\epsilon_d}{-\epsilon_m}\right)^{1/2}} \quad (6)$$

where K_0 is the propagation vector in free space, w is the width of the dielectric in MDM waveguide, λ is the wavelength of the EM wave, ϵ_d , ϵ_m are the permittivity of dielectric and metal respectively. The component of wave vector perpendicular to the

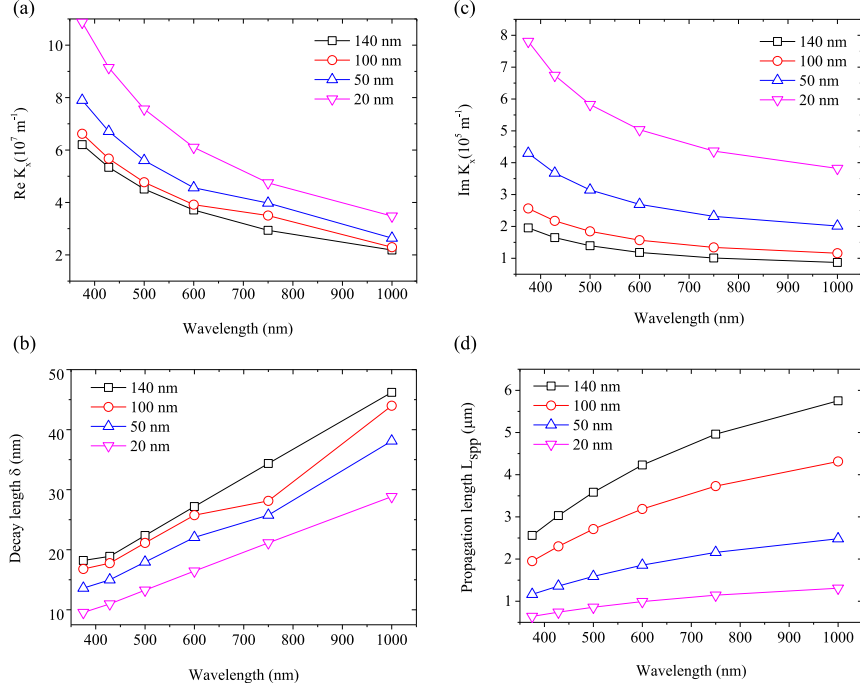


Figure 3. Surface plasmon polariton decay length (δ) and propagation length (L_{spp}) variation with dipole emitter wavelength for various dielectric-width (w) of the metal-dielectric-metal waveguide. (a) Real part of K_x vs dipole emitter wavelength, (b) Surface plasmon polariton decay length (δ) vs dipole emitter wavelength, (c) Imaginary part of K_x vs dipole emitter wavelength and (d) Surface plasmon polariton propagation length (L_{spp}) vs dipole emitter wavelength.

interface which quantifies the confinement of the wave can be calculated using K_{spp} as following [4].

$$K_y = \sqrt{K_{spp}^2 - \epsilon_d K_o^2} \quad (7)$$

The propagation length (L_{spp}) is defined as the distance by which the SPP field intensity drops to $1/e$, which is theoretically [4] given by $(2\text{Im}[K_{spp}])^{-1}$. The component of wave vector perpendicular to the interface defines another quantity called evanescent decay length [4], which is equal to $1/K_y$ and quantifies the confinement of the wave.

Fig. 2 (b) & (d) shows the simulation results for the transmission spectrum for various dielectric-width (w) ranging from 150 nm to 20 nm in steps of 10 nm. From the transmission vs wavelength plot, we find the wavelength for maximum transmission (λ_{max}). In Fig. 2 (d) we observe a shift in λ_{max} towards the smaller wavelength (blue shift) as the dielectric-width (w) is reduced continuously from 150 nm to 20 nm. To have a good trans-

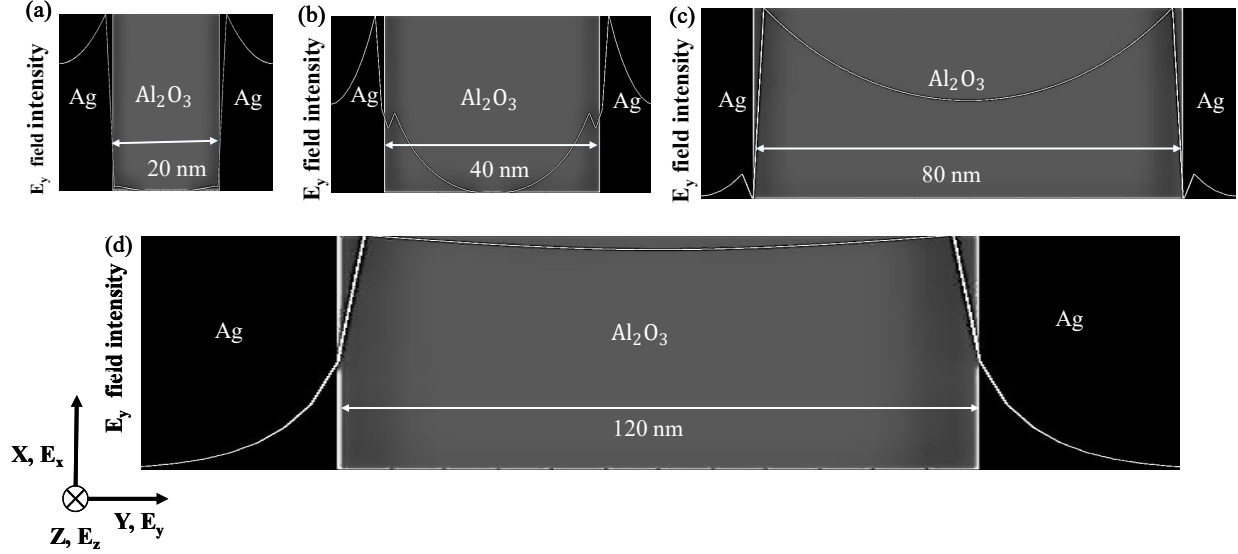


Figure 4. Transverse E_y field profile of the MDM waveguide for various dielectric width (w) and dipole emitter wavelength (λ). (a) $w = 20$ nm & $\lambda = 331$ nm, (b) $w = 40$ nm & $\lambda = 352$ nm, (c) $w = 80$ nm & $\lambda = 437$ nm and (d) $w = 120$ nm & $\lambda = 521$ nm.

mission rate for the MDM wave-guide we need a large value of propagation length and since propagation length decreases with reducing dielectric-width; we found that transmission too decreases with reducing dielectric-width. Once λ_{max} is known, we calculate the theoretical propagation length (L_{spp}) which is equal to $1/2\text{Im}[K_{spp}]$, from equation 6 and surface plasmon polariton decay length (δ) from the real part of K_{spp} using equation 7. The calculated values of L_{spp} and δ are plotted in Fig. 2 (c). From the FDTD simulation, we find that propagation length (L_{spp}) decreases with reducing w and for $w = 140$ nm the maximum propagation length (L_{spp}) of $3.98 \mu\text{m}$ is found. The theoretical calculation for L_{spp} is very close to the simulation results and the decay length (δ) gets as small as 9 nm for $w = 20$ nm. A similar relation was also shown in references, [7] and [50].

The effect of changing the dielectric-width (w) on the confinement and the propagation length for our Ag- Al_2O_3 -Ag MDM waveguide, has been studied using equation 6 [49]. From equation 6 and from Fig. 3, we observe that the $\text{Re}[K_{spp}]$ is inversely proportional to the dielectric-width (w), so the smaller the dielectric-width larger is the value of K . But we are not interested directly in the value of K_{spp} , what we want is a long propagation length and small decay length. Fig. 3 also plots the propagation length (L_{spp}) and decay length

Table I. Calculated values of key parameters for the analysis of SPP in the MDM waveguide such as effective mode length (L_{eff}), quality factor (Q), modal volume (V), group refractive index (n_g), plasmonic Purcell factor (F_p) and the coupling efficiency (β).

w (nm) ^a	λ_{max} (nm) ^b	δ (nm) ^c	L_{spp} (μm) ^d	L_{eff} (nm) ^e	Q ^f	V (nm ³) ^g	$\frac{V}{(\lambda/n)^3}$ ^h	n_g ⁱ	F_p ^j	β ^k
1	307*	1.726	0.1	0.863	58.32	149	0.0001	28.55	31974	99.99%
5	310*	3.91	0.231	1.958	60.83	1777	0.002	12.99	2879	99.96%
10	313*	5.64	0.342	2.823	64.03	5460	0.005	9.34	1022	99.90%
20	331	8.65	0.547	4.326	70.52	20498	0.015	4.81	249	99.60%
30	331	10.59	0.70	5.298	77.40	39445	0.029	3.75	129	99.23%
40	352	13.40	0.92	6.7011	84.54	82693	0.051	3.04	74.24	98.67%
50	352	14.98	1.072	7.492	91.71	120372	0.074	2.61	51.00	98.07%
60	376	18.06	1.331	9.032	99.37	217305	0.1103	2.24	34.43	97.17%
70	404	21.55	1.629	10.779	107.11	378626	0.15504	1.97	24.51	96.08%
80	437	25.62	1.974	12.814	114.74	648408	0.20978	1.76	18.11	94.76%
90	437	27.18	2.164	13.592	122.62	799868	0.25878	1.60	14.68	93.62%
100	475	31.97	2.576	15.989	130.04	1317242	0.33189	1.46	11.45	91.97%
110	521	37.97	3.051	18.878	136.672	2175310	0.41531	1.35	9.15	90.14%
120	521	39.43	3.280	19.718	144.754	2551046	0.48704	1.26	7.80	88.64%
130	576	46.47	3.840	23.238	150.203	4148286	0.58609	1.19	6.48	86.64%
140	576	48.23	4.091	24.115	158.26	4758647	0.67233	1.12	5.65	84.97%
150	644	57.09	4.750	28.546	161.75	7741885	0.78262	1.07	4.85	82.92%

^a w is the dielectric-width of the MDM waveguide in nm,

^b λ_{max} is the wavelength having maximum transmission for a fixed width of the MDM waveguide,

^c δ is the theoretical decay length in nm,

^d L_{spp} is the theoretical propagation length in μm , [L_{eff} is the effective mode length ($\delta/2$),

^f Q is the quality factor,

^g V is the modal volume of MDM waveguide,

^h $V/(\lambda/n)^3$ is the ratio of the modal volume in MDM waveguide to dielectric waveguide with n equal to refractive index of Al_2O_3 ,

ⁱ n_g is the group refractive index ($n_g \approx |n_{eff}|$),

^j F_p is the plasmonic Purcell factor and

^k β is the coupling efficiency.

The asterisk(*) values of λ_{max} have been computed by extrapolating the dielectric-width vs transmission λ_{max} plot.

(δ) for various dielectric-width and tells us that we can get good confinement by using smaller dielectric-width but at the same time will lose long propagation length. Hence it means that we cannot have the best of both the properties simultaneously. Although,

confinement of light beyond diffraction limit is advantageous for the field of plasmonics however a trade-off due to loss as a result of the confinement needs to be taken into account.

It is known that surface plasmon polaritons can only originate for the Transverse Magnetic (TM) mode of electromagnetic waves [4]. These TM plasmonic modes are characterized by the E_y field distribution as either symmetric mode TM_1 (even modes) or anti-symmetric mode TM_0 (odd modes). For TM_1 mode the E_y field is an even function with field maxima at each metal-dielectric interface and for TM_0 mode the E_y field is an odd function with field maxima at one metal-dielectric interface and field minima at another interface [4, 51]. Fig. 4 shows the transverse E_y field profile at the two interfaces which are symmetrical and hence the propagation mode is TM_1 . A similar pattern for the symmetric mode was also observed in Ref [51].

Using the calculated values for L_{spp} and δ , we derive the other key parameters for the analysis of SPP in the waveguide. These parameters are effective mode length (L_{eff}), quality factor (Q), modal volume (V), group refractive index (n_g), plasmonic Purcell factor (F_p) and the coupling efficiency (β) as shown in Table. I. The approach taken to calculate these parameters is discussed in Appendix D. The coupling efficiency ranges between 82 % to 99 % which is very efficient for the integration of SPS to nano waveguides. Coupling efficiency of quantum emitters and SPP strongly depends on dipole orientation. Maximum coupling was observed earlier [52] when dipole orientation is perpendicular the wave-guide axis (as is the case for our calculations i.e. in XY plane and along Y axis as shown in 1 a-b). Furthermore, the Bermudez et al [52] had shown that the coupling was shown to be zero when dipole was oriented along X and Z axis. The SPSs like WSe₂, hBN (hexagonal Boron Nitride), MoS₂ monolayer and NV (Nitrogen Vacancy) center in nanodiamond crystals can be integrated deterministically by all-dry viscoelastic stamping [53]. Deterministic integration of SPS to plasmonic waveguide has been shown by several researchers [52, 54–59]. Along with the coupling of SPS to a plasmonic waveguide, minimum loss and good confinement are also required for integrated photonic devices. For dielectric waveguides, the mode volume is the order of $(\frac{\lambda_0}{n})^3$ where n is the refractive index of the medium. But for our plasmonic waveguide, the modal volume ranges between 0.01 % to 78 % of $(\frac{\lambda_0}{n})^3$ which is very smaller than that for the dielectric waveguide & hence proves the subwavelength confinement of the mode. The plasmonic Purcell fac-

tor is found to be inversely proportional to modal volume (V) and ranging between 4 to 31974 for various dielectric-width as shown in Table I.

CALCULATION FOR INDISTINGUISHABILITY & EXTRACTION EFFICIENCY

One can achieve good extraction efficiency and indistinguishability by coupling the SPS with a nanoplasmonic cavity which is evanescently coupled to the SPP plasmonic mode of the waveguide. Spontaneous emission by vacuum fluctuations for a two-level quantum system exhibits pure indistinguishable photons. Often the dephasing takes place which relates to the quantum decoherence, and in that case the indistinguishability is represented by the following equation

$$I = \frac{\gamma}{\gamma + \gamma^*} \quad (8)$$

where γ represents the quantum emitter decay rate and the γ^* the dephasing rate [60]. The value for γ^* is around $10^4 \gamma$, hence it can be seen from the formula that indistinguishability is very low, of the order of 10^{-4} , for an emitter in free space or not coupled to a cavity. [34, 65]. However, coupling SPS inside an optical cavity results in an increase of both the extraction efficiency and the indistinguishability [65, 74–76], the increment in I is due to the modification of the local density of the electromagnetic states (LDOS). In the cavity quantum electrodynamics (cavity-QED) picture, the relevant parameters for the drastic change in the indistinguishability are the emitter-cavity coupling rate (g), κ the cavity decay rate and Q the quality factor [34, 60, 65]. The approach taken to calculate these parameters is discussed in Appendix E.

Many researchers have probed the use of nanoplasmonic cavities and antennas to enhance the light-matter interactions using structures such as bow-tie antenna and NPoM (nanoparticle on a mirror) coupled with SPSs [77, 90–95]. We have calculated the indistinguishability and extraction efficiency for SPSs coupled with an NPoM plasmonic cavity as fabricated in [77] which in turn is coupled evanescently with our MDM waveguide. The NPoM cavity consists of a spherical gold nanoparticle of 40 nm diameter on the top of a 70 nm thick gold film separated by a 0.9 nm molecular spacer [77, 96]. We have assumed that the cavity and emitter are resonant with each other making $\omega_c = \omega_e$. As the plasmonic cavity, we have selected the NPoM because it is possible to change the reso-

Table II. Literature survey of Indistinguishability (I), efficiency (η) and the dephasing rate γ^* for various categories of SPS

Category of SPS	I	η	γ^*
Self assembled InAs/GaAs quantum dots coupled to a photonic crystal cavity [60]	72%	8.8 %	116.6 γ
Single silicon vacancy (SiV) center in a nano-diamond coupled to a fiber cavity [60]	81%	3.5%	3437.5 γ
Colloidal quantum dots in coupled cavities (optimal) [34]	90%	0.24%	83000 γ
Colloidal quantum dots in coupled cavities (experimental) [34]	63%	0.15%	83000 γ
GaAs QD [61, 62]	90%	-	-
GaAs with new broadband photonic structure, CBR-HBR ^a [63]	90%	85%	-
InGaAs QD coupled to elliptical micro pillars Bragg Grating devices [64]	97%	60%	-
Si vacancy center in diamond at room temperature with cascaded cavity systems [65]	31.5%	98.7%	10 ⁴ γ
Quantum dots coupled to single/multimode -ridged waveguide [66]	95%/97.5%	-	-
BBO(Barium borate)-SPDC source [67]	83%	-	-
Si vacancy center in diamond, (5 K) [68]	72%	-	-
Atom-cavity system (Rb atom - cavity) [69]	90%	-	-
Dibenzanthanthrene (DBATT) molecule incorporated in Shpolskii matrices of n-tetradecane [70]	-	30%	-
WSe ₂ monolayer onto a SiN waveguide [71]	7%	93%	-
Potassium titanyl phosphate (aKTP) crystal- parametric downconversion (PDC) source [72]	98%	-	-
Quantum dots coupled to a cavity (4 K) [73]	99%	96%	-

^a CBR-HBR : Circular Bragg resonators on highly efficient broadband reflectors

Table IV. Values of various key parameters for the analysis of SPS and nanoplasmonic cavity coupled system.

SPS ^a	λ (nm) ^b	Q ^c	p_d (D) ^d	g (THz) ^e	κ (THz) ^f	γ (MHz) ^g	γ^* (MHz) ^h	R (THz) ⁱ	I ^j	η^k	$(I \times \eta)^l$
Methylene blue* ^[77]	665	15.9	3.8 ^[77]	82.44	178	15.34	$\gamma \times 10^4$	152.44	0.9987	0.9998	0.9985
CsPbI ₃ * ^[78]	660	8	3.5 ^[79]	71.26	356	13.31	$\gamma \times 10^4$	56.904	0.9907	0.9999	0.9906
CdSe ^[80]	510	8	10 ^[81]	230	461	235.61	$\gamma \times 10^2$	458	0.9999	0.9999	0.9998
InGaAlAs ^[82]	680	8	29 ^[83]	582	346	835.96	$\gamma \times 10^2$	3911	0.9996	0.9999	0.9995
WSe ₂ ^[84]	713	8	16 ^[85]	518	330	220.74	$\gamma \times 10^2$	3249	0.9999	0.9999	0.9998
InGaN ^[86]	450	8	21 ^[87]	312	523	1512.58	$\gamma \times 10^2$	743	0.9996	0.9999	0.9995
hBN ^[88]	594	8	0.65 ^[88]	13.94	396	0.6291	$\gamma \times 10^4$	1.961	0.9873	0.9979	0.9852
NV in diamond ^[89]	637	8	1.3 ^[89]	26.94	369	2.03	$\gamma \times 10^4$	7.86	0.9898	0.9995	0.9893

^a SPS is the Single Photon Source,

^b λ is the wavelength of the mentioned SPS,

^c Q is the quality factor,

^d p_d is the dipole moment strength for the SPS shown in D (Debye) which is equal to 3.3×10^{-30} C.m,

^e g is the emitter cavity coupling rate,

^f κ is the cavity decay rate,

^g γ is the emitter decay rate,

^h γ^* is the decoherence rate,

ⁱ R is the population transfer rate between emitter and cavity,

^j I is the indistinguishability,

^k η is the extraction efficiency and

^l $I \times \eta$ is the product of indistinguishability (I) and efficiency η , which should be 1 for an ideal SPS.

nant wavelength of the cavity by changing the shape and size of the nanoparticle in the plasmonic cavity ^[77].

The SPSs we have used for the calculations are methylene blue single molecule ^[77], CsPbI₃^[78], hexagonal Boron Nitride (hBN) ^[88], CdSe ^[80], InGaAlAs ^[82], InGaN ^[86], WSe₂ ^[84] and Nitrogen vacancy (NV) in diamonds ^[89]; out of these Methylene blue, CsPbI₃, NV in diamond & hBN are room-temperature single-photon sources (γ^* of the order of 10^4 times γ) while the rest require a cryogenic set up to operate as SPS(γ^* of the

order of 10^2 times γ). For the calculation of indistinguishability (I), we have kept the quality factor (Q) equal to 8 and modal volume (V) equal to 40 nm^3 for all the SPS, apart from the methylene blue for which the values quoted in Chikkaraddy et.al.[77] have been used which are $Q = 15.9$ and $V = 35 \text{ nm}^3$. For the NPoM cavity we found that the Purcell factor is of the order of 10^6 . For all these SPSs the emitter wavelength and the cavity decay rate (κ) is shown in Table. IV. The emitter cavity coupling strength "g" is calculated using the dipole strength (p_d) as quoted in Table. IV, keeping $\cos\theta_d$ as 1. From the calculated values of κ , γ and γ^* and g, we found that quantum emitters such as methylene blue single molecule, CdSe, InGaAlAs, WSe₂, and InGaAlAs are in the strong coupling regime and CsPbI₃, hexagonal Boron Nitride (hBN) and Nitrogen Vacancy (NV) in diamond are in the weak coupling regime. Our calculated value of $2g$ for methylene blue single molecule matches with the experimental value of rabi splitting as quoted in [77]. The valuee for γ , the emitter decay rate was calculated using the transition rate formula given by Fermi's golden rule [97] & γ^* the dephasing rate is taken as 100 times γ for low temperature (4K) [71] and 10000 times γ for room temperature [60]. We have calculated the values for I & η as shown in Table. IV for both strong and weak coupling using the equations for indistinguishability and extraction efficiency as discussed in Appendix E. For both the case of strong and weak coupling in cavity-emitter system, we find that I and η are close to 99 %. These values are adequately high as compared to the emitters reported earlier in the Table II. We believe this makes these emitters better SPS to be used for quantum technology application. The increase in the single photon indistinguishability and extraction efficiency for a weak coupling between the cavity and emitter is due to the high Purcell factor for the plasmonic cavities. Switching from weak coupling regime to the strong coupling results in an increase in the Purcell factor (F_p) as F_p is directly proportional to g^2 . However for strong coupling there is an upper bound on the effect of Purcell factor on the indistinguishability and extraction efficieny due to the clamping of the effective decay rate of the quantum dot[98]. The use of strong coupling regime between emitter and cavity to enhance the single photon properties has been experimentally reported in [99–101].

QUANTUM INFORMATION PROCESSING

Mach-Zehnder interferometer circuits using MDM waveguide and single photons can lead to quantum computers [102]. Using nonlinear Kerr medium (Fig. 5, red region) such as MEH-PPV [poly(2-methoxy-5-(28-ethylhexyloxy)-PPV)] having $n_2 1.8 \times 10^{-13} \text{cm}^2 / \text{W}$ at 1064 nm wavelength [39, 103] and InAs quantum dots [104] phase shift $\Delta \Phi$ pf (π) can be achieved. On-resonant quantum dots and cavity in one arm can also lead to the phase shift of π [105]. For cross-phase modulation (XPM), the relative phase shift of π in both arms require firstly, one of the arms to be longer. Secondly, the nonlinear materials hold have larger nonlinear susceptibilities χ^3 , and thirdly, the sources of the single photons should be brighter to enhance the intensity (I) dependent refractive index ($\Delta n = n_2 I$), n_2 is a nonlinear coefficient. Our metal-dielectric-metal waveguide serves longer surface plasmon polariton propagation length helping solve the first problem. Choosing higher non-linear coefficient (n_2) materials will solve the second problem. While Purcell enhanced single-photon source, for example, bow tie or NPoM coupled SPS is a potential candidate for brighter and faster single-photon source solving the third problem. Our proposed scheme to build quantum logic circuits using a nanoantenna enhanced SPS is shown in Fig. 5.

CONCLUSION

In conclusion, the operation of plasmonic waveguide based on SPP in photonic integrated circuits has been studied. The key parameters that are needed for full-scale implementation of plasmonic waveguides such as propagation length, decay length, coupling efficiency (between the waveguide and quantum emitter), and plasmonic Purcell factor for MDM waveguide have been analyzed using FDTD simulations and analytical methods. We found the coupling efficiency to be greater than 82% for dielectric-width (w) in the range of 20 nm - 150 nm and the plasmonic Purcell factor increasing with decreasing w , reaching as high as 31974 for $w = 1$ nm from 4.85 for $w = 150$ nm. We found the maximum propagation length (L_{spp}) of $3.98 \mu\text{m}$ from the simulations for dielectric-width equal to 140 nm at λ equal to 576 nm. Along with this, we found that the decay length (δ) is directly proportional to the dielectric-width of the MDM waveguide and ranges be-

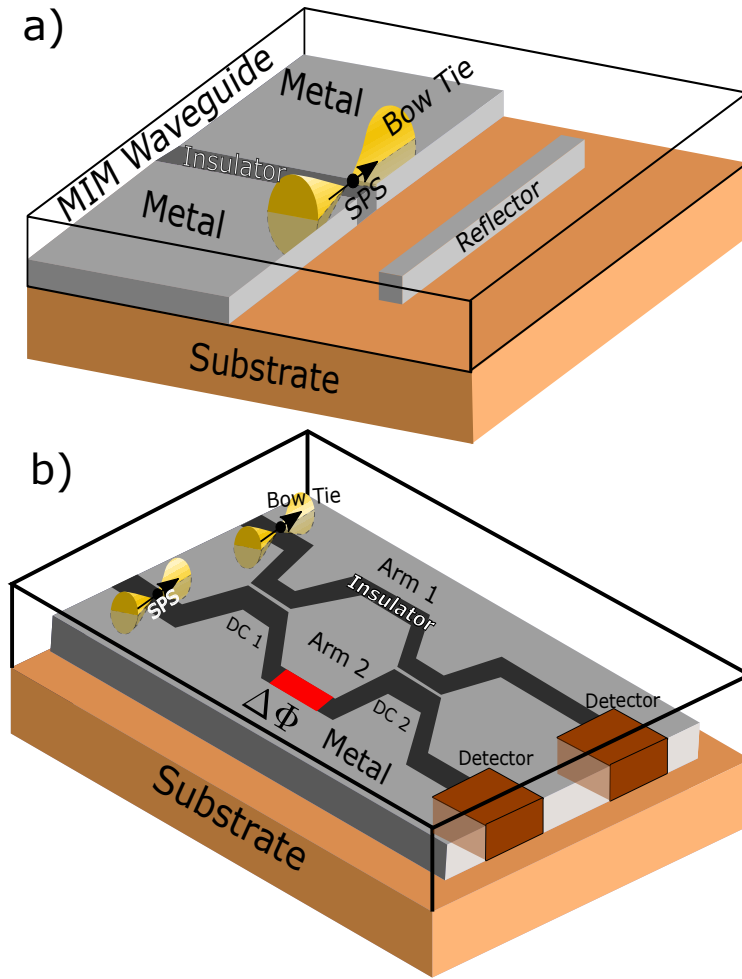


Figure 5. a) Proposed schematics for a quantum logic circuit: Deterministically placed hybrid bow-tie nanoantenna single photon sources (SPS) in a metal-dielectric-metal(MIM) waveguide. b) Mach-Zehnder interferometer acting as controlled quantum logic gate, deterministically placed antenna-SPS metal-dielectric-metal waveguide sends polarized qubits, directional couplers (DC1 and DC2) acting as the beam splitter process the information and qubit is registered by single photon detector (superconducting nanowires etc). The phase shift $\Delta \Phi$ is introduced by a non-linear material placed inside the wave guide (red region).

tween 8 nm to 60 nm for w between 20 nm - 150 nm respectively. Hence it is clear that there exists a trade-off between localization and loss in plasmonic waveguides; the better the confinement (smaller decay length), the lower is the propagation length. We also studied the effect on the indistinguishability (I) and extraction efficiency (η) for several single-photon sources coupled with the NPoM plasmonic cavity. And found indistin-

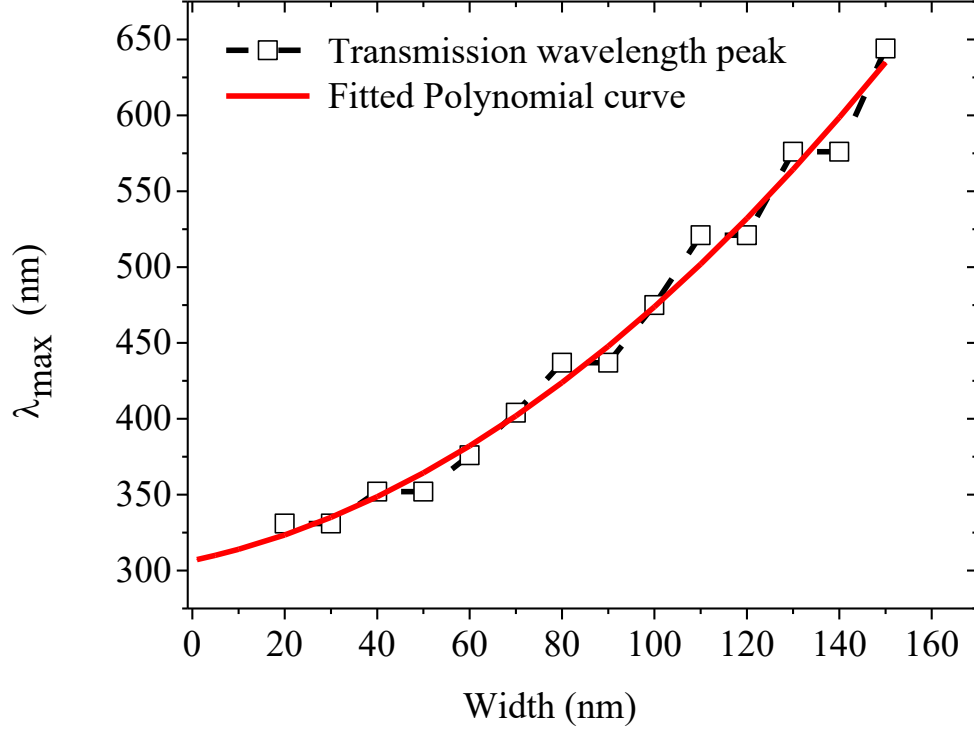


Figure 6. Interpolation plot for width vs Transmission λ_{max} .

guishability close to 99 % at room temperature and extraction efficiency (η) around 99 %. We also proposed the design of a quantum logic gate based on a deterministically placed nano-plasmonic antenna-SPS coupled system with a metal-dielectric-metal waveguide.

ACKNOWLEDGMENT

We acknowledge Birla Institute of Technology, Mesra, Ranchi, and the Ministry of Human Resource Development, Government of India, for support through TEQIP-III and Collaborative Research Scheme (CRS): CRS-ID:1-5736483014. We are thankful to Subham Adak for useful discussion and Kostav Konar for technical help.

Interpolation plot for finding the transmission λ_{max} values for width 1 nm, 5 nm and 10 nm

In Table. I of the paper the asterisk(*) values of λ_{max} have been found using the following interpolation plot. From the Fig. 6 we get

$$\lambda_{max} = 306.55 + (0.63w) + (0.01033w^2) \quad (9)$$

where w is the width and using w as 1 nm, 5 nm and 10 nm gives λ_{max} as 307 nm, 310 nm and 313 nm respectively.

Condition for surface plasmon polariton propagation

Typically, used metals for the study of surface plasmon polariton are gold (Au) and silver (Ag). Both these metal are chemically inert, stable, shows excellent tailorable binding to bio-molecules and also have low loss compared to other metals. In this study, we have used Ag which has plasma energy of 9.013 eV ($\omega_p = 1.37 \times 10^4$ THz) [47] and collision frequency γ of around 100 THz [4]. The dielectric function of Ag as described by Drude model is [1, 46]

$$\epsilon(\omega) = 1 - \frac{\omega_p^2}{\omega^2 + i\gamma\omega} \quad (10)$$

The complex dielectric function of Ag has been plotted in Fig. 7, along with the dielectric constant for Al_2O_3 which is 9. For $\omega < \omega_p$, the real part of the dielectric constant for Ag is negative as it must be for the existence of SPPs and the imaginary part is positive which corresponds to energy loss of propagating SPPs. For electromagnetic waves with $\omega > \omega_p$, we have a positive ϵ and hence the electromagnetic waves do not get shielded. So the waves with $\omega > \omega_p$ can propagate in the metal. The value of ω_p for metals lies in the ultra-violet range and the dispersion relation for the waves having $\omega > \omega_p$ is given by

$$\omega^2 = \omega_p^2 + c^2 K^2 \quad (11)$$

The plot of ω and K can be seen in Fig. 2 (a) of the paper.

Simulation results for 100 nm dielectric-width MDM waveguide showing its propagation properties and E field vs Wavelength profile

For the FDTD simulation the source of the electromagnetic radiation used was a total scattered wave, for which we have selected the range between 100 to 1000 nm. A point size electric field monitor was used to simulate the E field. In Fig. 8 the E field vs wavelength profile is plotted; the highest peak is at λ equal 437 nm and the lower peak at λ equal to 170 nm. The resonance around 437 nm corresponds to the SPP mode of the MDM waveguide. For $w = 100$ nm, the diffraction limit as calculated by $d \approx \lambda/2$ would give λ

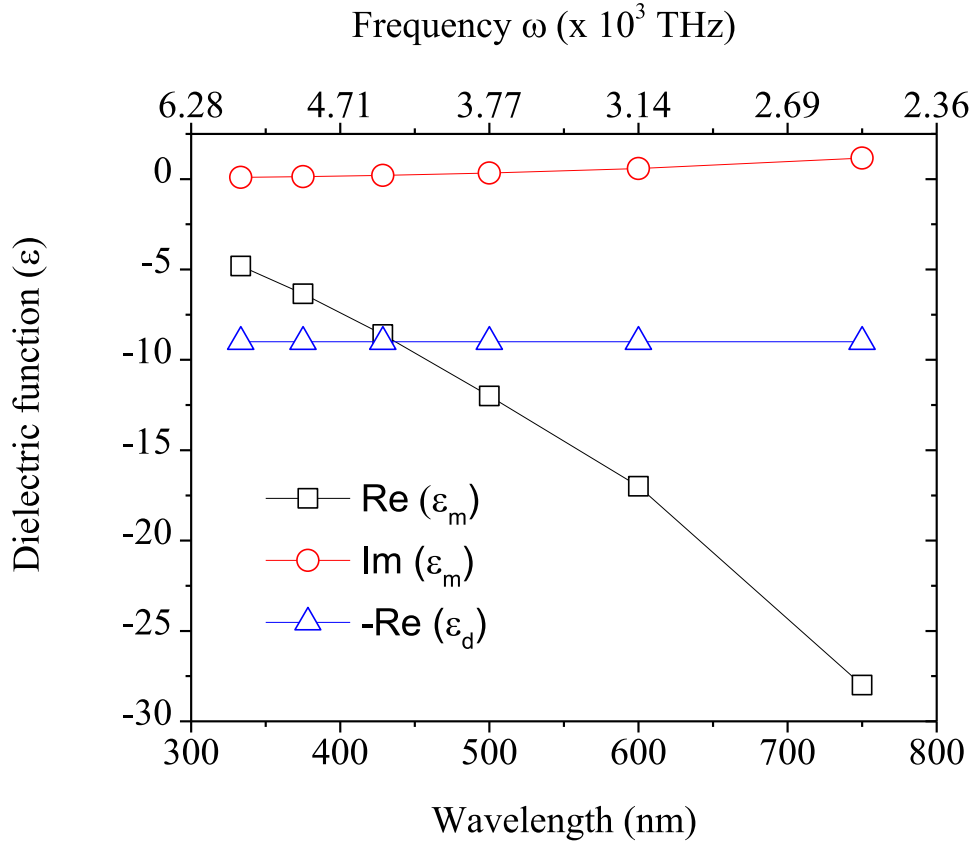


Figure 7. Plot of the complex dielectric function for silver and negative of the dielectric constant value for Al_2O_3 .

≈ 200 nm which is very close to the second peak observed at 170 nm which lies in the UV range of the EM spectrum. Along with the field vs wavelength profile, we also simulated the E_x field variation in the propagating direction which is the X-axis. In Fig. 9 the results of this simulation have been plotted for the two peak wavelength, 170 nm & 437 nm. The propagation length (L_{spp}) is defined as the distance by which the E-field intensity in the propagation direction drops to $1/e$ (36.78 %) of its maximum value. For 100 nm dielectric width of the MDM waveguide at dipole emitter wavelength equal to 437 nm we found that the L_{spp} is equal to $2.6 \mu\text{m}$.

The Fig. 10 shows the simulation results for X-Y field profile; (a) X-Y field profile showing the surface waves (SPP) propagating in the x-direction at $\lambda = 437$ nm for 100 nm dielectric-width MDM waveguide and (b) X-Y field profile showing the wave propagation at $\lambda = 170$ nm for 100 nm dielectric-width MDM waveguide.

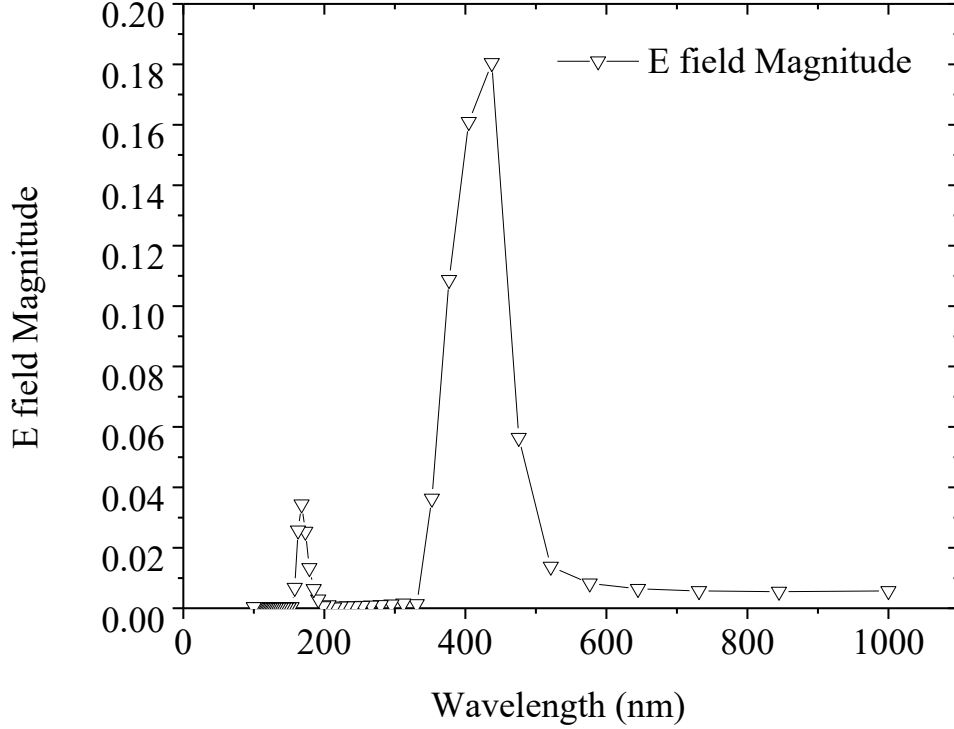


Figure 8. The E field Vs Wavelength profile with SPP peak at λ equal to 437 nm, for 100 nm dielectric-width MDM waveguide.

Calculation of key parameters for the analysis of SPP in the waveguide

The environment of a quantum emitter (SPS) alter its spontaneous emission rate given by the Purcell Factor

$$F_p = \frac{3}{4\pi^2} \left(\frac{Q}{V_c}\right) \left(\frac{\lambda}{n}\right)^3 \quad (12)$$

Consequently, it's clear that by increasing quality factor (Q) and by lowering the mode volume (V_c) we can substantially increase the Purcell factor. The Purcell factor (F_p) as shown in equation 12 quantifies the emission enhancement of light in an emitter-cavity system. The phenomenon of confinement of light energy in a volume much below the diffraction limit of $(\lambda_0/2n)^3$ [4] (where n is the refractive index of the dielectric) in SPP modes also leads to a very small modal volume.

The SPP quality factor Q is defined as the following [106].

$$Q = K_{spp} / \Delta(K_{spp}) \approx K_{spp} L_{spp} \quad (13)$$

where K_{spp} represents the SPP wavevector in the propagation direction and ΔK_{spp} rep-

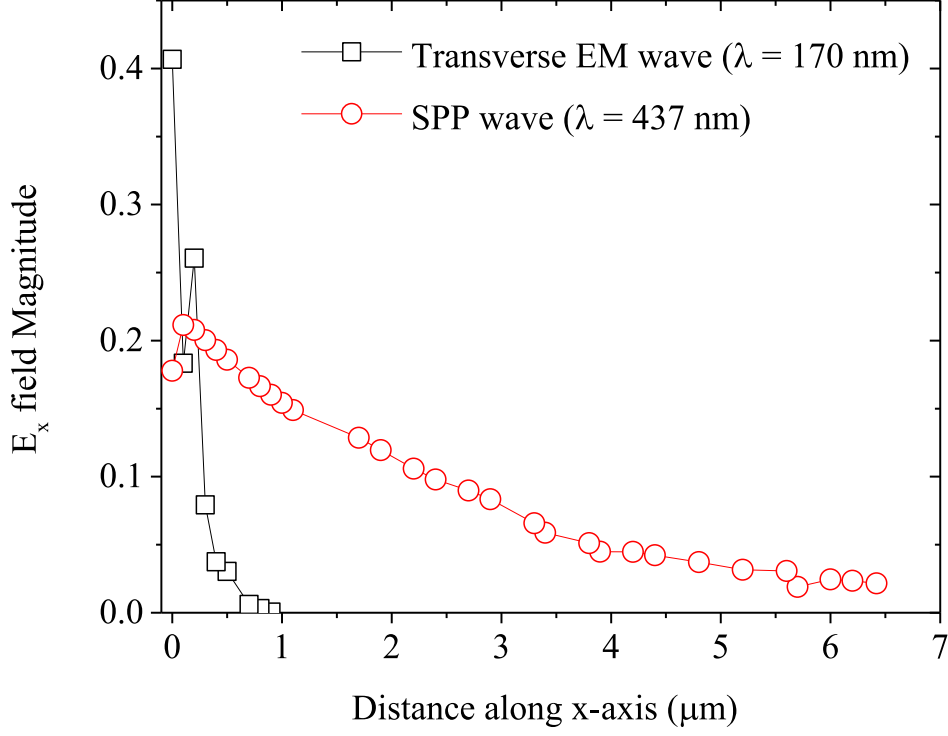


Figure 9. E_x field vs distance along x-axis plot for the MDM waveguide showing the propagation property of the SPP for the 100 nm dielectric width MDM waveguide at λ equal to 437 nm.

resents the imaginary part of it. The mode volume V for a plasmonic waveguide is [106].

$$V = A_{eff} 2L_{spp} \quad (14)$$

where L_{spp} is the propagation length and A_{eff} is the effective mode area, which is the measure of the area which a waveguide mode covers in the transverse direction. For SPP modes the transverse direction is same as the direction of the confinement of the mode which is represented by the effective mode length [106]

$$L_{eff} = \frac{\int |(E(z))|^2 dz}{\text{Max} |(E(z))|^2} = \int_0^\infty e^{-2z/\delta} dz = \delta/2 \quad (15)$$

where δ is the surface plasmon polariton decay length. In terms of effective length we can write the effective mode area A_{eff} as $(L_{eff})^2$. The plasmonic Purcell factor for a plasmonic waveguide can thus be defined as [106]

$$F_p = \frac{3}{4\pi^2} \left(\frac{\lambda_{em}}{n_1}\right)^3 \frac{Q_{spp}}{V} \frac{\omega_{em}}{V_g K_{spp}} \quad (16)$$

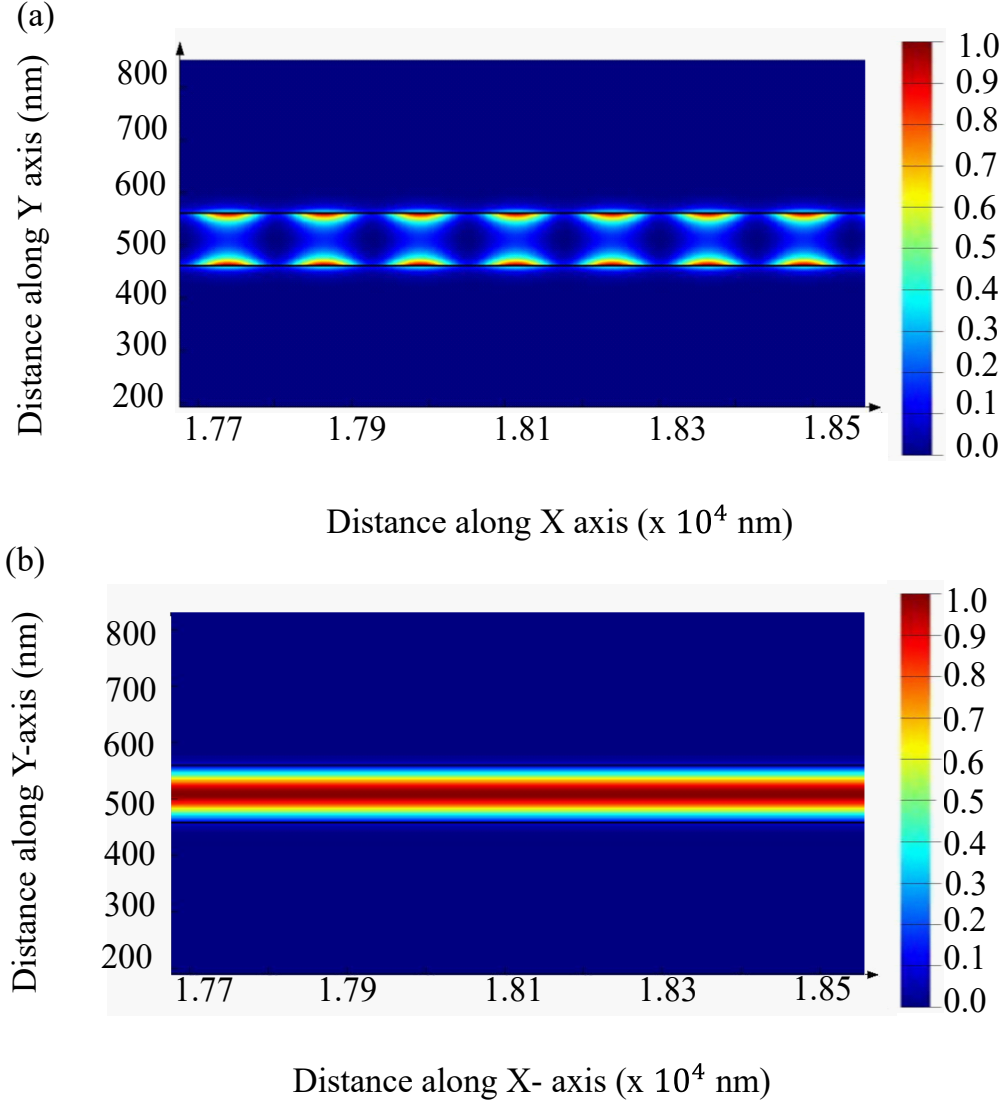


Figure 10. X-Y field profile of the MDM waveguide for dielectric width (w) equal to 100 nm. (a) Field profile at $\lambda = 437$ nm & (b) Field profile at $\lambda = 170$ nm. The color scale bar represents the normalized field intensity.

where Q_{spp} is the quality factor, V is the modal volume of the plasmonic waveguide as defined by equation 14, n_1 is the refractive index of the dielectric material, V_g is the group velocity of SPP. The group velocity (V_g) can be calculated by taking the inverse of $\frac{dK_{spp}}{d\omega}$. And substituting all the above described factors we get the following formula for the plasmonic Purcell factor [106].

$$F_p = \frac{3}{4\pi} \frac{(\lambda_{em}/n_1)^2 n_g}{A_{eff} n_1} \quad (17)$$

where n_g is the group refractive index of the confined mode and n_1 is the refractive index

of the dielectric medium [106]. For the practical use of plasmonic waveguide in photonic integrated circuits, the coupling of emitted energy from the dipole or the SPS to the waveguide modes has to be very high. Using the plasmonic Purcell factor we can estimate the coupling efficiency between the dipole emitter and the waveguide modes. The equation for coupling efficiency (β) in terms of Purcell factor is given by [106].

$$\beta \approx \frac{F_p}{1 + F_p} \quad (18)$$

Cavity QED picture: Calculation of Indistinguishability and Efficiency

The quantum emitter decay rate γ has been calculated using the transition rate given by the Fermi's golden rule [97]

$$\gamma = \frac{p_d^2 \omega^3}{3\pi\epsilon_0 \hbar c^3} \quad (19)$$

where p_d , ω are the dipole moment and angular frequency of the emitter respectively.

The emitter- cavity coupling rate (g) is given by [60]

$$g = \cos \theta_d \frac{1}{\sqrt{V_c}} p_d \sqrt{\frac{\omega_c}{2\hbar\epsilon_0}} \quad (20)$$

Here V_c is the cavity mode volume, p_d is the strength of the dipole moment of the emitter, θ_d is the angle between the unit polarization vector of the emitter e_d and the cavity field vector e_c . The cavity decay rate κ is given by

$$\kappa = \omega_c / Q \quad (21)$$

where ω_c is the cavity resonant frequency and Q is the cavity quality factor. Based on the values for g , κ , γ , and γ^* we can categorize the emitter-cavity coupling in two parts, the strong coupling & the weak coupling. If $4|g| > |\kappa - \gamma - \gamma^*|$ then the emitter - cavity coupling is referred to as strong coupling and if $4|g| < |\kappa - \gamma - \gamma^*|$ then it is case the weak coupling [99, 101, 107, 108]. For the strong coupling regime the indistinguishability is represented by the following formula [60].

$$I = \frac{(\gamma + \kappa)(\gamma + \kappa + \gamma^*/2)}{(\gamma + \kappa + \gamma^*)^2} \quad (22)$$

And in the weak coupling regime, if we have $\kappa > \gamma + \gamma^*$ then it's the bad cavity regime for which indistinguishability is I_{BC} which is represented by the following formula [60].

$$I_{BC} = \frac{\gamma + R}{\gamma + R + \gamma^*} \quad (23)$$

where R (population transfer rate between emitter and the cavity) is given by

$$R = \frac{4g^2}{\gamma + \kappa + \gamma^*} \quad (24)$$

The theoretical extraction efficiency for both the cases is represented by the following formula [60, 109]

$$\eta = \frac{\kappa R}{(\kappa R) + (\gamma(\kappa + R))} \quad (25)$$

* nara.laxmi@gmail.com

- [1] H. Yang, J. Li, G. Xiao, Decay and propagation properties of symmetric surface plasmon polariton mode in metal–insulator–metal waveguide, *Opt. Commun.* 395 (2017) 159–162. [doi:10.1016/j.optcom.2015.10.057](https://doi.org/10.1016/j.optcom.2015.10.057).
- [2] Z. Han, S. I. Bozhevolnyi, Waveguiding with surface plasmon polaritons, in: *Modern Plasmonics*, Elsevier, 2014, pp. 137–187. [doi:10.1016/b978-0-444-59526-3.00005-7](https://doi.org/10.1016/b978-0-444-59526-3.00005-7).
- [3] S. I. Bozhevolnyi, Effective-index modeling of channel plasmon polaritons, *Opt. Express* 14 (20) (2006) 9467. [doi:10.1364/oe.14.009467](https://doi.org/10.1364/oe.14.009467).
- [4] S. A. Maier, *Plasmonics: Fundamentals and Applications*, Springer Science & Business Media, 2007.
- [5] V. E. Babicheva, R. Malureanu, A. V. Lavrinenko, Plasmonic finite-thickness metal–semiconductor–metal waveguide as ultra-compact modulator, *Photonics Nanostruct. Fundam. Appl.* 11 (4) (2013) 323–334. [doi:10.1016/j.photonics.2013.07.009](https://doi.org/10.1016/j.photonics.2013.07.009).
- [6] A. Boltasseva, T. Nikolajsen, K. Leosson, K. Kjaer, M. Larsen, S. Bozhevolnyi, Integrated optical components utilizing long-range surface plasmon polaritons, *J. Light. Technol.* 23 (1) (2005) 413–422. [doi:10.1109/jlt.2004.835749](https://doi.org/10.1109/jlt.2004.835749).
- [7] J. A. Dionne, L. A. Sweatlock, H. A. Atwater, A. Polman, Planar metal plasmon waveguides: frequency-dependent dispersion, propagation, localization, and loss beyond the free electron model, *Phys. Rev. B* 72 (7) (aug 2005). [doi:10.1103/physrevb.72.075405](https://doi.org/10.1103/physrevb.72.075405).
- [8] E. Ozbay, Plasmonics: Merging photonics and electronics at nanoscale dimensions, *Science* 311 (5758) (2006) 189–193. [doi:10.1126/science.1114849](https://doi.org/10.1126/science.1114849).
- [9] R. Zia, J. Schuller, A. Chandran, M. Brongersma, Plasmonics: the next chip-scale technology, *Mater. Today* 9 (7-8) (2006) 20–27. [doi:10.1016/S1369-7021\(06\)71572-3](https://doi.org/10.1016/S1369-7021(06)71572-3).

- [10] R. Zia, M. D. Selker, P. B. Catrysse, M. L. Brongersma, Geometries and materials for sub-wavelength surface plasmon modes., *J. Opt. Soc. Am. A Opt. Image Sci. Vis.* 21 (12) (2004) 2442–2446.
- [11] Y. Fang, M. Sun, Nanoplasmonic waveguides: towards applications in integrated nanophotonic circuits, *Light Sci. Appl.* 4 (2015) e294. doi:10.1038/lssa.2015.67.
- [12] Y. Matsuzaki, T. Okamoto, M. Haraguchi, M. Fukui, M. Nakagaki, Characteristics of gap plasmon waveguide with stub structures, *Opt. Express* 16 (21) (2008) 16314. doi:10.1364/oe.16.016314.
- [13] Y. Bian, Q. Gong, Compact all-optical interferometric logic gates based on one-dimensional metal–insulator–metal structures, *Opt. Commun.* 313 (2014) 27–35. doi:10.1016/j.optcom.2013.09.055.
- [14] Y. Kurokawa, H. T. Miyazaki, Metal-insulator-metal plasmon nanocavities: Analysis of optical properties, *Phys. Rev. B* 75 (3) (jan 2007). doi:10.1103/physrevb.75.035411.
- [15] V. Caligiuri, M. Palei, G. Biffi, S. Artyukhin, R. Krahne, A semi-classical view on epsilon-near-zero resonant tunneling modes in metal/insulator/metal nanocavities, *Nano Lett.* 19 (5) (2019) 3151–3160. doi:10.1021/acs.nanolett.9b00564.
- [16] J. B. Khurgin, G. Sun, Practicality of compensating the loss in the plasmonic waveguides using semiconductor gain medium, *Appl. Phys. Lett.* 100 (1) (2012) 011105. doi:10.1063/1.3673849.
- [17] Y. C. Jun, R. D. Kekatpure, J. S. White, M. L. Brongersma, Nonresonant enhancement of spontaneous emission in metal-dielectric-metal plasmon waveguide structures, *Phys. Rev. B* 78 (15) (2008) 153111. doi:10.1103/PhysRevB.78.153111.
- [18] R. Faggiani, J. Yang, P. Lalanne, Quenching, plasmonic, and radiative decays in nanogap emitting devices, *ACS Photonics* 2 (12) (2015) 1739–1744. doi:10.1021/acsp Photonics.5b00424.
- [19] T. Søndergaard, J. Jung, S. I. Bozhevolnyi, G. D. Valle, Theoretical analysis of gold nanostrip gap plasmon resonators, *New J. Phys.* 10 (10) (2008) 105008. doi:10.1088/1367-2630/10/10/105008.
- [20] G. Veronis, S. H. Fan, Guided subwavelength plasmonic mode supported by a slot in a thin metal film, *Opt. Lett.* 30 (24) (2005) 3359–3361. doi:10.1364/OL.30.003359.
- [21] J. A. Dionne, H. J. Lezec, H. A. Atwater, Highly confined photon transport in sub-

- wavelength metallic slot waveguides, *Nano Lett.* 6 (9) (2006) 1928–1932. doi:10.1021/nl0610477.
- [22] J. A. Dionne, L. A. Sweatlock, H. A. Atwater, A. Polman, Plasmon slot waveguides: Towards chip-scale propagation with subwavelength-scale localization, *Phys. Rev. B* 73 (3) (2006) 035407. doi:10.1103/PhysRevB.73.035407.
- [23] S. I. Bozhevolnyi, V. S. Volkov, E. Devaux, J.-Y. Laluet, T. W. Ebbesen, Channel plasmon subwavelength waveguide components including interferometers and ring resonators., *Nature* 440 (7083) (2006) 508–511. doi:10.1038/nature04594.
- [24] W. Cai, M. L. Brongersma, Plasmonics gets transformed, *Nat. Nanotechnol.* 5 (7) (2010) 485–486. doi:10.1038/nano.2010.140.
- [25] A. Chandran, E. S. Barnard, J. S. White, M. L. Brongersma, Metal-dielectric-metal surface plasmon-polariton resonators, *Phys. Rev. B* 85 (8) (2012) 085416. doi:10.1103/PhysRevB.85.085416.
- [26] W. L. Barnes, A. Dereux, T. W. Ebbesen, Surface plasmon subwavelength optics, *Nature* 424 (6950) (2003) 824–830. doi:10.1038/nature01937.
- [27] E. Knill, R. Laflamme, G. J. Milburn, A scheme for efficient quantum computation with linear optics, *Nature* 409 (6816) (2001) 46–52. doi:10.1038/35051009.
- [28] Y. He, Y.-M. He, Y.-J. Wei, X. Jiang, M.-C. Chen, F.-L. Xiong, Y. Zhao, C. Schneider, M. Kamp, S. Höfling, C.-Y. Lu, J.-W. Pan, Indistinguishable tunable single photons emitted by spin-flip raman transitions in InGaAs quantum dots., *Phys. Rev. Lett.* 111 (2013) 237403. doi:10.1103/PhysRevLett.111.237403.
- [29] L. N. Tripathi, O. Iff, S. Betzold, U. Dusanowski, M. Emmerling, K. Moon, Y. J. Lee, S.-H. Kwon, S. Höfling, C. Schneider, Spontaneous emission enhancement in strain-induced WSe₂ monolayer-based quantum light sources on metallic surfaces, *ACS Photonics* 5 (5) (2018) 1919–1926, publication Date (Web): April 4, 2018. doi:10.1021/acsp Photonics.7b01053.
- [30] A. Sajid, M. Ford, J. Reimers, Single-photon emitters in hexagonal boron nitride: a review of progress, *Rep. Prog. Phys.* 83 (4), (2020). doi:10.1088/1361-6633/ab6310.
- [31] G. Grosso, H. Moon, B. Lienhard, S. Ali, D. K. Efetov, M. M. Furchi, P. Jarillo-Herrero, M. J. Ford, I. Aharonovich, D. Englund, Tunable and high-purity room temperature single-photon emission from atomic defects in hexagonal boron nitride., *Nat. Commun.* 8 (2017)

705. doi:10.1038/s41467-017-00810-2.
- [32] S. K. H. Andersen, S. Kumar, S. I. Bozhevolnyi, Ultrabright linearly polarized photon generation from a nitrogen vacancy center in a nanocube dimer antenna, *Nano Lett.* 17 (6) (2017) 3889–3895. doi:10.1021/acs.nanolett.7b01436.
- [33] M. D. Eisaman, J. Fan, A. Migdall, S. V. Polyakov, Invited review article: Single-photon sources and detectors, *Rev. Sci. Instrum.* 82 (7) (2011) 071101. doi:10.1063/1.3610677.
- [34] A. Saxena, Y. Chen, A. Ryou, C. G. Sevilla, P. Xu, A. Majumdar, Improving indistinguishability of single photons from colloidal quantum dots using nanocavities, *ACS Photonics* (nov 2019). doi:10.1021/acsp Photonics.9b01481.
- [35] Y.-M. He, Y. He, Y.-J. Wei, D. Wu, M. Atatüre, C. Schneider, S. Höfling, M. Kamp, C.-Y. Lu, J.-W. Pan, On-demand semiconductor single-photon source with near-unity indistinguishability, *Nat. Nanotechnol.* 8 (3) (2013) 213–217.
- [36] X. Ding, Y. He, Z.-C. Duan, N. Gregersen, M.-C. Chen, S. Unsleber, S. Maier, C. Schneider, M. Kamp, S. Höfling, C.-Y. Lu, J.-W. Pan, On-demand single photons with high extraction efficiency and near-unity indistinguishability from a resonantly driven quantum dot in a micropillar., *Phys. Rev. Lett.* 116 (2) (2016) 20401.
- [37] G. Veronis, S. Fan, Bends and splitters in metal-dielectric-metal subwavelength plasmonic waveguides, *Appl. Phys. Lett.* 87 (13) (2005) 131102. doi:10.1063/1.2056594.
- [38] G. Veronis, S. Fan, Theoretical investigation of compact couplers between dielectric slab waveguides and two-dimensional metal-dielectric-metal plasmonic waveguides, *Opt. Express* 15 (3) (2007) 1211–1221. doi:10.1364/OE.15.001211.
- [39] M. Pu, N. Yao, C. Hu, X. Xin, Z. Zhao, C. Wang, X. Luo, Directional coupler and nonlinear mach-zehnder interferometer based on metal-insulator-metal plasmonic waveguide, *Opt. Express* 18 (20) (2010) 21030–21037. doi:10.1364/OE.18.021030.
- [40] J. O’Brien, A. Furusawa, J. Vučković, Photonic quantum technologies, *Nat. Photonics* 3 (12) (2009) 687–695. doi:10.1038/nphoton.2009.229.
- [41] T. Vogl, M. Doherty, B. Buchler, Y. Lu, P. Lam, Atomic localization of quantum emitters in multilayer hexagonal boron nitride, *Nanoscale* 11 (30) (2019) 14362–14371. doi:10.1039/c9nr04269e.
- [42] W. K. Wootters, W. H. Zurek, *A single quantum cannot be cloned*, *Nature* 299 (5886) (1982) 802–803.

- [43] M. Krenn, M. Malik, T. Scheidl, R. Ursin, A. Zeilinger, Quantum communication with photons, in: *Optics in Our Time*, Springer International Publishing, 2016, pp. 455–482.
- [44] P. P. Rohde, J. P. Dowling, The on-ramp to the all-optical quantum information processing highway, *Science* 349 (6249) (2015) 696–696. doi:10.1126/science.aac7250.
- [45] J. Carolan, C. Harrold, C. Sparrow, E. Martín-López, N. Russell, J. Silverstone, P. Shadbolt, N. Matsuda, M. Oguma, M. Itoh, G. Marshall, M. Thompson, J. Matthews, T. Hashimoto, J. O’Brien, A. Laing, Universal linear optics, *Science* 349 (6249) (2015) 711–716. doi:10.1126/science.aab3642.
- [46] P. B. Johnson, R. W. Christy, Optical constants of noble metals, *Phys. Rev. B* 6 (12) (1972) 4370–4379. doi:10.1103/PhysRevB.6.4370.
- [47] L. J. M. Herrera, D. M. Arboleda, D. C. Schinca, L. B. Scaffardi, [Determination of plasma frequency, damping constant, and size distribution from the complex dielectric function of noble metal nanoparticles](#), *J. Appl. Phys.* 116 (23) (2014) 233105. doi:10.1063/1.4904349.
- [48] J. Robertson, High dielectric constant oxides, *Eur. Phys. J. AP* 28 (3) (2004) 265–291. doi:10.1051/epjap:2004206.
- [49] S. Collin, F. Pardo, J.-L. Pelouard, [Waveguiding in nanoscale metallic apertures](#), *Opt. Express* 15 (7) (2007) 4310. doi:10.1364/oe.15.004310.
- [50] M. T. Noghani, M. H. V. Samiei, Propagation characteristics of multilayer hybrid insulator-metal-insulator and metal-insulator-metal plasmonic waveguides, *Adv. Electromagn.* 2 (3) (2014) 35. doi:10.7716/aem.v2i3.222.
- [51] J. A. Dionne, L. A. Sweatlock, M. T. Sheldon, A. P. Alivisatos, H. A. Atwater, Silicon-based plasmonics for on-chip photonics, *IEEE Journal of Selected Topics in Quantum Electronics* 16 (1) (2010) 295–306. doi:10.1109/jstqe.2009.2034983.
- [52] E. Bermúdez-Ureña, C. Gonzalez-Ballester, M. Geiselmann, R. Marty, I. P. Radko, T. Holmgaard, Y. Alaverdyan, E. Moreno, F. J. García-Vidal, S. I. Bozhevolnyi, R. Quidant, Coupling of individual quantum emitters to channel plasmons, *Nat. Commun.* 6 (1) (2015) 7883. doi:10.1038/ncomms8883.
- [53] A. Castellanos-Gomez, M. Buscema, R. Molenaar, V. Singh, L. Janssen, H. S. J. van der Zant, G. A. Steele, Deterministic transfer of two-dimensional materials by all-dry viscoelastic stamping, *2D Mater.* 1 (1) (2014) 011002. doi:10.1088/2053-1583/1/1/011002.
- [54] H. Siampour, S. Kumar, S. I. Bozhevolnyi, Chip-integrated plasmonic cavity-enhanced sin-

- gle nitrogen-vacancy center emission, *Nanoscale* 9 (45) (2017) 17902–17908. doi:10.1039/c7nr05675c.
- [55] M. Blauth, J. Harms, M. Prechtel, J. J. Finley, M. Kaniber, Enhanced optical activity of atomically thin MoSe₂ proximal to nanoscale plasmonic slot-waveguides, *2d Mater.* 4 (2) (2017) 021011. doi:10.1088/2053-1583/aa52b0.
- [56] H. Siampour, S. Kumar, S. I. Bozhevolnyi, Nanofabrication of plasmonic circuits containing single photon sources, *ACS Photonics* 4 (8) (2017) 1879–1884. doi:10.1021/acsp Photonics.7b00374.
- [57] H. Siampour, S. Kumar, V. A. Davydov, L. F. Kulikova, V. N. Agafonov, S. I. Bozhevolnyi, On-chip excitation of single germanium vacancies in nanodiamonds embedded in plasmonic waveguides, *Light Sci. Appl.* 7 (1) (sep 2018). doi:10.1038/s41377-018-0062-5.
- [58] T. Cai, S. Dutta, S. Aghaeimeibodi, Z. Yang, S. Nah, J. Fourkas, E. Waks, Coupling emission from single localized defects in 2d semiconductor to surface plasmon polaritons, *Nano Lett.* 17 (11) (2017) 6564–6568. doi:10.1021/acs.nanolett.7b02222.
- [59] S. Dutta, T. Cai, M. A. Buyukkaya, S. Barik, S. Aghaeimeibodi, E. Waks, Coupling quantum emitters in WSe₂ monolayers to a metal-insulator-metal waveguide, *Appl. Phys. Lett.* 113 (19) (2018) 191105. doi:10.1063/1.5045727.
- [60] T. Grange, G. Hornecker, D. Hunger, J.-P. Poizat, J.-M. Gérard, P. Senellart, A. Auffèves, Cavity-funneled generation of indistinguishable single photons from strongly dissipative quantum emitters, *Phys. Rev. Lett.* 114 (19) (may 2015). doi:10.1103/physrevlett.114.193601.
- [61] M. Reindl, J. H. Weber, D. Huber, C. Schimpf, S. F. C. da Silva, S. L. Portalupi, R. Trotta, P. Michler, A. Rastelli, Highly indistinguishable single photons from incoherently excited quantum dots, *Phys. Rev. B* 100 (15) (oct 2019). doi:10.1103/physrevb.100.155420.
- [62] C. Nawrath, F. Olbrich, M. Paul, S. L. Portalupi, M. Jetter, P. Michler, Coherence and indistinguishability of highly pure single photons from non-resonantly and resonantly excited telecom c-band quantum dots, *Appl. Phys. Lett.* 115 (2) (2019) 023103. doi:10.1063/1.5095196.
- [63] J. Liu, R. Su, Y. Wei, B. Yao, S. F. C. da Silva, Y. Yu, J. Iles-Smith, K. Srinivasan, A. Rastelli, J. Li, X. Wang, A solid-state source of strongly entangled photon pairs with high brightness and indistinguishability, *Nat. Nanotechnol.* 14 (6) (2019) 586–593. doi:10.1038/

[s41565-019-0435-9](#).

- [64] H. Wang, Y.-M. He, T.-H. Chung, H. Hu, Y. Yu, S. Chen, X. Ding, M.-C. Chen, J. Qin, X. Yang, R.-Z. Liu, Z.-C. Duan, J.-P. Li, S. Gerhardt, K. Winkler, J. Jurkat, L.-J. Wang, N. Gregersen, Y.-H. Huo, Q. Dai, S. Yu, S. Höfling, C.-Y. Lu, J.-W. Pan, Towards optimal single-photon sources from polarized microcavities, *Nat. Photonics* 13 (11) (2019) 770–775. [doi:10.1038/s41566-019-0494-3](#).
- [65] H. Choi, D. Zhu, Y. Yoon, D. Englund, Cascaded cavities boost the indistinguishability of imperfect quantum emitters, *Phys. Rev. Lett.* 122 (18) (may 2019). [doi:10.1103/physrevlett.122.183602](#).
- [66] Ł. Dusanowski, S.-H. Kwon, C. Schneider, S. Höfling, Near-unity indistinguishability single photon source for large-scale integrated quantum optics, *Phys. Rev. Lett.* 122 (17) (may 2019). [doi:10.1103/physrevlett.122.173602](#).
- [67] R. Kaltenbaek, B. Blauensteiner, M. Żukowski, M. Aspelmeyer, A. Zeilinger, Experimental interference of independent photons, *Phys. Rev. Lett.* 96 (24) (jun 2006). [doi:10.1103/physrevlett.96.240502](#).
- [68] A. Sipahigil, K. Jahnke, L. Rogers, T. Teraji, J. Isoya, A. Zibrov, F. Jelezko, M. Lukin, Indistinguishable photons from separated silicon-vacancy centers in diamond, *Phys. Rev. Lett.* 113 (11) (sep 2014). [doi:10.1103/physrevlett.113.113602](#).
- [69] T. Legero, T. Wilk, M. Hennrich, G. Rempe, A. Kuhn, Quantum beat of two single photons, *Phys. Rev. Lett.* 93 (7) (aug 2004). [doi:10.1103/physrevlett.93.070503](#).
- [70] V. Ahtee, R. Lettow, R. Pfab, A. Renn, E. Ikonen, S. Götzinger, V. Sandoghdar, Molecules as sources for indistinguishable single photons, *J. Mod. Opt.* 56 (2-3) (2009) 161–166. [doi:10.1080/09500340802464657](#).
- [71] F. Peyskens, C. Chakraborty, M. Muneeb, D. V. Thourhout, D. Englund, Integration of single photon emitters in 2d layered materials with a silicon nitride photonic chip, *Nat. Commun.* 10 (1) (sep 2019). [doi:10.1038/s41467-019-12421-0](#).
- [72] F. Graffitti, P. Barrow, M. Proietti, D. Kundys, A. Fedrizzi, Independent high-purity photons created in domain-engineered crystals, *Optica* 5 (5) (2018) 514. [doi:10.1364/optica.5.000514](#).
- [73] J. Iles-Smith, D. P. S. McCutcheon, A. Nazir, J. Mørk, [Phonon scattering inhibits simultaneous near-unity efficiency and indistinguishability in semiconductor single-photon sources](#),

- Nat. Photonics 11 (8) (2017) 521–526. doi:10.1038/nphoton.2017.101.
- [74] O. Gazzano, S. Michaelis de Vasconcellos, C. Arnold, A. Nowak, E. Galopin, I. Sagnes, L. Lanco, A. Lemaître, P. Senellart, [Bright solid-state sources of indistinguishable single photons](#), Nat. Commun. 4 (2013) 1425.
- [75] J. M. Gerard, B. Sermage, B. Gayral, B. Legrand, E. Costard, V. Thierry-Mieg, Enhanced spontaneous emission by quantum boxes in a monolithic optical microcavity, Phys. Rev. Lett. 81 (5) (1998) 1110–1113. doi:10.1103/PhysRevLett.81.1110.
- [76] R. Albrecht, A. Bommer, C. Deutsch, J. Reichel, C. Becher, Coupling of a single nitrogen-vacancy center in diamond to a fiber-based microcavity, Phys. Rev. Lett. 110 (24) (jun 2013). doi:10.1103/physrevlett.110.243602.
- [77] R. Chikkaraddy, B. de Nijs, F. Benz, S. J. Barrow, O. A. Scherman, E. Rosta, A. Demetriadou, P. Fox, O. Hess, J. J. Baumberg, Single-molecule strong coupling at room temperature in plasmonic nanocavities, Nature 535 (7610) (2016) 127–130. doi:10.1038/nature17974.
- [78] Y.-S. Park, S. Guo, N. S. Makarov, V. I. Klimov, Room temperature single-photon emission from individual perovskite quantum dots, ACS Nano 9 (10) (2015) 10386–10393. doi:10.1021/acsnano.5b04584.
- [79] J.-K. Sun, S. Huang, X.-Z. Liu, Q. Xu, Q.-H. Zhang, W.-J. Jiang, D.-J. Xue, J.-C. Xu, J.-Y. Ma, J. Ding, Q.-Q. Ge, L. Gu, X.-H. Fang, H.-Z. Zhong, J.-S. Hu, L.-J. Wan, Polar solvent induced lattice distortion of cubic CsPbI₃ nanocubes and hierarchical self-assembly into orthorhombic single-crystalline nanowires, J. Am. Chem. Soc. 140 (37) (2018) 11705–11715. doi:10.1021/jacs.8b05949.
- [80] T. Aichele, V. Zwiller, O. Benson, Visible single-photon generation from semiconductor quantum dots, New J. Phys. 6 (2004) 90–90. doi:10.1088/1367-2630/6/1/090.
- [81] T. Nakabayashi, R. Ohshima, N. Ohta, Electric field effects on photoluminescence of CdSe nanoparticles in a PMMA film, Crystals 4 (2) (2014) 152–167. doi:10.3390/cryst4020152.
- [82] M. V. Rakhlin, K. G. Belyaev, G. V. Klimko, I. S. Mukhin, S. V. Ivanov, A. A. Toropov, [Single-photon emission from InAs/AlGaAs quantum dots](#), Phys. Solid State 60 (4) (2018) 691–694. doi:10.1134/S1063783418040261.
- [83] P. G. Eliseev, H. Li, A. Stintz, G. T. Liu, T. C. Newell, K. J. Malloy, L. F. Lester, Transition dipole moment of InAs/InGaAs quantum dots from experiments on ultralow-threshold laser diodes, Appl. Phys. Lett. 77 (2) (2000) 262–264. doi:10.1063/1.126944.

- [84] M. Koperski, K. Nogajewski, A. Arora, V. Cherkez, P. Mallet, J. Y. Veuillen, J. Marcus, P. Kosacki, M. Potemski, Single photon emitters in exfoliated WSe₂ structures, *Nat. Nanotechnol.* 10 (6) (2015) 503–506. doi:10.1038/NNANO.2015.67.
- [85] C. Jin, J. Kim, K. Wu, B. Chen, E. S. Barnard, J. Suh, Z. Shi, S. G. Drapcho, J. Wu, P. J. Schuck, S. Tongay, F. Wang, On optical dipole moment and radiative recombination lifetime of excitons in WSe₂, *Adv. Funct. Mater.* 27 (19) (2016) 1601741. doi:10.1002/adfm.201601741.
- [86] S. Deshpande, J. Heo, A. Das, P. Bhattacharya, Electrically driven polarized single-photon emission from an InGaN quantum dot in a GaN nanowire, *Nat. Commun.* 4 (1) (apr 2013). doi:10.1038/ncomms2691.
- [87] I. A. Ostapenko, G. Hönig, C. Kindel, S. Rodt, A. Strittmatter, A. Hoffmann, D. Bimberg, Large internal dipole moment in InGaN/GaN quantum dots, *Appl. Phys. Lett.* 97 (6) (2010) 063103. doi:10.1063/1.3477952.
- [88] Y. Xia, Q. Li, J. Kim, W. Bao, C. Gong, S. Yang, Y. Wang, X. Zhang, Room-temperature giant stark effect of single photon emitter in van der waals material., *Nano letters* (Sep. 2019). doi:10.1021/acs.nanolett.9b02640.
- [89] P. Tamarat, T. Gaebel, J. R. Rabeau, M. Khan, A. D. Greentree, H. Wilson, L. C. L. Hollenberg, S. Praver, P. Hemmer, F. Jelezko, J. Wrachtrup, Stark shift control of single optical centers in diamond, *Phys. Rev. Lett.* 97 (2006) 083002. doi:10.1103/PhysRevLett.97.083002.
- [90] N. Kongsuwan, A. Demetriadou, R. Chikkaraddy, F. Benz, V. A. Turek, U. F. Keyser, J. J. Baumberg, O. Hess, Suppressed quenching and strong-coupling of purcell-enhanced single-molecule emission in plasmonic nanocavities, *ACS Photonics* 5 (1) (2017) 186–191. doi:10.1021/acsphotonics.7b00668.
- [91] D. E. Chang, A. S. Sørensen, E. A. Demler, M. D. Lukin, A single-photon transistor using nanoscale surface plasmons, *Nat. Phys.* 3 (11) (2007) 807–812.
- [92] M.-E. Kleemann, R. Chikkaraddy, E. M. Alexeev, D. Kos, C. Carnegie, W. Deacon, A. C. de Pury, C. Große, B. de Nijs, J. Mertens, A. I. Tartakovskii, J. J. Baumberg, Strong-coupling of WSe₂ in ultra-compact plasmonic nanocavities at room temperature, *Nat. Commun.* 8 (1) (nov 2017). doi:10.1038/s41467-017-01398-3.
- [93] X. Fang, L. Hu, K. Huo, B. Gao, L. Zhao, M. Liao, P. K. Chu, Y. Bando, D. Golberg, New ultraviolet photodetector based on individual Nb₂O₅ nanobelts, *Adv. Funct. Mater.* 21 (20) (2011) 3907–3915. doi:10.1002/adfm.201100743.

- [94] D. Conteduca, C. Reardon, M. G. Scullion, F. Dell’Olio, M. N. Armenise, T. F. Krauss, C. Ciminelli, Ultra-high Q/V hybrid cavity for strong light-matter interaction, *APL Photonics* 2 (8) (2017) 086101. doi:10.1063/1.4994056.
- [95] G. Lu, J. Liu, T. Zhang, H. Shen, P. Perriat, M. Martini, O. Tillement, Y. Gu, Y. He, Y. Wang, Q. Gong, Enhancing molecule fluorescence with asymmetrical plasmonic antennas, *Nanoscale* 5 (14) (2013) 6545–6551. doi:10.1039/c3nr01306e.
- [96] P. K. Aravind, H. Metiu, Use of a perfectly conducting sphere to excite the plasmon of a flat surface. 1. calculation of the local field with applications to surface-enhanced spectroscopy, *The Journal of Physical Chemistry* 86 (26) (1982) 5076–5084. doi:10.1021/j100223a007.
- [97] M. Fox, *Quantum optics: an introduction*, Vol. 15, OUP Oxford, 2006.
- [98] P. Kaer, N. Gregersen, J. Mork, The role of phonon scattering in the indistinguishability of photons emitted from semiconductor cavity QED systems, *New J. Phys.* 15 (3) (2013) 035027. doi:10.1088/1367-2630/15/3/035027.
- [99] S. Gerhardt, M. Deppisch, S. Betzold, T. H. Harder, T. C. H. Liew, A. Predojević, S. Höfling, C. Schneider, Polarization-dependent light-matter coupling and highly indistinguishable resonant fluorescence photons from quantum dot-micropillar cavities with elliptical cross section, *Phys. Rev. B* 100 (11) (sep 2019). doi:10.1103/physrevb.100.115305.
- [100] K. Hennessy, A. Badolato, M. Winger, D. Gerace, M. Atatuer, S. Gulde, S. Faelt, E. L. Hu, A. Imamoglu, Quantum nature of a strongly coupled single quantum dot-cavity system, *Nature* 445 (7130) (2007) 896–899. doi:10.1038/nature05586.
- [101] D. Press, S. Götzinger, S. Reitzenstein, C. Hofmann, A. Löffler, M. Kamp, A. Forchel, Y. Yamamoto, Photon antibunching from a single quantum-dot-microcavity system in the strong coupling regime, *Phys. Rev. Lett.* 98 (11) (mar 2007). doi:10.1103/physrevlett.98.117402.
- [102] I. L. C. Michael A. Nielsen, *Quantum Computation and Quantum Information*, Cambridge University Pr., 2010.
- [103] M. A. Bader, G. Marowsky, A. Bahtiar, K. Koynov, C. Bubeck, H. Tillmann, H.-H. Hörhold, S. Pereira, Poly(p-phenylenevinylene) derivatives: new promising materials for nonlinear all-optical waveguide switching, *J. Opt. Soc. Am. B* 19 (9) (2002) 2250. doi:10.1364/josab.19.002250.
- [104] H. Nakamura, Y. Sugimoto, K. Kanamoto, N. Ikeda, Y. Tanaka, Y. Nakamura, S. Ohkouchi, Y. Watanabe, K. Inoue, H. Ishikawa, K. Asakawa, Ultra-fast photonic crystal/quantum dot

- all-optical switch for future photonic networks, *Opt. Express* 12 (26) (2004) 6606–6614.
- [105] P. Androvitsaneas, A. Young, J. Lennon, C. Schneider, S. Maier, J. Hinchliff, G. Atkinson, E. Harbord, M. Kamp, S. Höfling, J. Rarity, R. Oulton, Efficient quantum photonic phase shift in a low q-factor regime, *ACS Photonics* 6 (2) (2019) 429–435. doi:[10.1021/acsp Photonics.8b01380](https://doi.org/10.1021/acsp Photonics.8b01380).
- [106] G. C. des Francs, J. Barthes, A. Bouhelier, J. C. Weeber, A. Dereux, A. Cuche, C. Girard, Plasmonic purcell factor and coupling efficiency to surface plasmons. implications for addressing and controlling optical nanosources, *J. Opt.* 18 (9) (2016) 094005. doi:[10.1088/2040-8978/18/9/094005](https://doi.org/10.1088/2040-8978/18/9/094005).
- [107] T. Huemmer, F. J. Garcia-Vidal, L. Martin-Moreno, D. Zueco, Weak and strong coupling regimes in plasmonic qed, *Phys. Rev. B* 87 (11) (2013) 115419. doi:[10.1103/PhysRevB.87.115419](https://doi.org/10.1103/PhysRevB.87.115419).
- [108] G.-C. Shan, Z.-Q. Yin, C. H. Shek, W. Huang, Single photon sources with single semiconductor quantum dots, *Front. Phys.* 9 (2) (2013) 170–193. doi:[10.1007/s11467-013-0360-6](https://doi.org/10.1007/s11467-013-0360-6).
- [109] A. Auffèves, D. Gerace, J.-M. Gérard, M. F. Santos, L. C. Andreani, J.-P. Poizat, Controlling the dynamics of a coupled atom-cavity system by pure dephasing, *Phys. Rev. B* 81 (24) (jun 2010). doi:[10.1103/physrevb.81.245419](https://doi.org/10.1103/physrevb.81.245419).